Geophysics Exploration using Gravity Gradients

Sali Wolobah (wolobah@aims.ac.za)
African Institute for Mathematical Sciences (AIMS)

Supervised by Robert de Mello Koch and Neil Pendock
University of Witwatersrand

June 8, 2007

Abstract

A promising modern approach to geophysics exploration involves airborne gravity surveys. The gradient of the gravitational field (in general, this is a tensor with 6 independent components) is measured. A proper description of the gradient field sourced by the terrain is obtained by developing the Green's function for the gravity gradient field . This also allows us to formulate the problem in an effective dipole model. The effective dipole description may provide a more efficient appreach to the forward modelling problem. Before the number of corrections are necessary . These descriptions are described in detail. An important source of noise in this data arises due to aircraft motion.

Contents

1. Introduction

Potentials play an important role in geophysics because they describe the behaviour of gravitational fields. In this report the measurement of the gravitational fields and gravitational gradients during airborne surveys provide important information on the gravitational potential. This we demonstrate in Chapter 2. These same measurements can help in determining the imprint of mass distribution at the Earth's surface. These measurements are accomplished by means of a gradiometer and gravimeter mounted on the aircraft that flies above sea level. Theoretically, Laplace's Equation and Poisson's equation are used to analyze and determine the mass distribution giving rise to these measurements.

Poisson's equation can be solved using the Green's function technique. This we demonstrate in Chapter 1. In essence the derivation of the Green's function yields the well known result that the gravitational potential for a point mass M is given by $-\gamma M/r$ where γ is the Universal Gravitational Constant, and r is the separation between the point mass and the point of observation.

Prior to geophysical interpretation of measurement data, a so called Digital Terrain Model representing the local terrain is proposed and used to efficiently compute the gravitational gradient. These computations form part of the so called Bouguer Gravity Correction, which is often applied to remove the high degree of correlation of the free air gravity anomaly with terrain elevation. Thus in areas of very flat relief, the Simple Bouguer Correction is usually all that is required. However, in areas of rugged local relief accurate geophysical interpretation requires the use of the Complete Bouguer correction and hence the computations using the Digital Terrain Models. This correction and others are the subject of Chapter 3.

We give a conclusion of all these discussions in Chapter 4.

2. The Concept of Green's Function

2.1 Green's Function for Ordinary Differential Equations

In this section we introduce the concept of the Green's function in the context of solving a linear inhomogeneous ordinary differential equation (ODE). Ultimately our goal is to solve Poisson's equation using the Green's function method which we do in Section 2.2. The main result of this section is the equation which will determine the Green's function for a linear ODE.

Let us consider the general form of a linear inhomogeneous ordinary differential equation:

$$a_n(x)\frac{d^n y}{dx^n} + \cdots + a_1(x)\frac{dy}{dx} + a_0(x)y = f(x). \tag{2.1}$$

We can express the above equation as follows:

$$\mathcal{L}y(x) = f(x), \tag{2.2}$$

where $\mathcal{L}$ is the linear operator:

$$a_n(x)\frac{d^n}{dx^n} + \cdots + a_1(x)\frac{d}{dx} + a_0(x) \ . \tag{2.3}$$

Let us suppose that a function $G(x, z)$ exists such that the general solution of Equation (2.2) holds for an imposed boundary condition in the range $a \leq x \leq b$ and can be written as

$$y(x) = \int_a^b G(x, z)f(x)dz. \tag{2.4}$$

Equation (2.4) defines $G(x, z)$ as the Green's function for the ODE (2.2). Applying the linear operator $\mathcal{L}$ to the both sides of Equation (2.4) and using Equation (2.2) we then obtain:

$$\mathcal{L}y(x) = \int_a^b \mathcal{L}G(x, z)f(z)dz = f(x). \tag{2.5}$$

From the standard property of Dirac's delta function,

$$f(x) = \int_a^b \delta(x - z)f(z)dz, \tag{2.6}$$

we deduce that

$$\mathcal{L}G(x, z) = \delta(x - z). \tag{2.7}$$

Thus we require that the Green's function $G(x, z)$ must satisfy the orginal ODE (2.2) with the RHS set to Dirac's delta function. We can also deduce from Equation (2.4) that if $y(x)$ is to satisfy the imposed boundary conditions, then $G(x, z)$ must also satisfy these boundary conditions.

Physically, $G(x, z)$ may be thought of as the response of a system at the point x due to a unit impulse at z.

2.2 Green's Function for Poisson's Equation

Poisson's equation is important in calculating the gravitational potential, $U(\mathbf{r})$, the gravitational field, $\mathbf{g}(\mathbf{r}) = -\nabla U$, and the gravity gradient, $[g_{ij}] = \nabla\nabla U$ (see Section 3.1). In this section we introduce Poisson's equation and determine its Green's function for use in calculating the gravitational potential.

Poisson's equation is a partial differential equation (PDE) whose solution gives the gravitational potential, $U(\mathbf{r})$, due to a mass density distribution, $\rho(\mathbf{r})$. Poisson's equation is

$$\nabla^2 U(\mathbf{r}) = 4\pi\gamma\rho(\mathbf{r}) \tag{2.8}$$

where γ is the gravitational constant.

Clearly, Poisson's equation reduces to Laplace's equation for $\rho(\mathbf{r}) = 0$.

We wish to solve Poisson's equation in some region V bounded by a surface ∂V. We seek a solution for U that satisfies the PDE and the boundary condition that U is zero at infinity. In this case the volume V is infinite but is treated formally by taking the surface ∂V as a large sphere of radius R and letting R tend to infinity.

In order to solve Poisson's equation subject to the boundary conditions mentioned above we will use *Green's second theorem* which state that for two scalar functions ϕ and $\psi(r)$ defined in some volume V bounded by a surface ∂V,

$$\int_V (\phi\nabla^2\psi - \psi\nabla^2\phi)\, dV = \int_{\partial V} (\phi\nabla\psi - \psi\nabla\phi)\cdot\hat{\mathbf{n}}\, d(\partial V), \tag{2.9}$$

where on the RHS it is common to write, for example, $\nabla\psi\cdot\hat{\mathbf{n}}d(\partial V)$ as $(\partial\psi/\partial n)\, d(\partial V)$. The expression $(\partial\psi/\partial n)$ stands for $\nabla\psi\cdot\hat{\mathbf{n}}$, the rate of change of ψ in the direction of the unit outward normal $\hat{\mathbf{n}}$ to the surface ∂V.

The Green's function for Poisson's equation must satisfy

$$\frac{1}{4\pi\gamma}\nabla^2 G(\mathbf{r},\mathbf{r}_0) = \delta(r - r_0), \tag{2.10}$$

where $\mathbf{r}_0$ lies in V. (As mentioned above, we may think of $G(\mathbf{r},\mathbf{r}_0)$ as the solution to Poisson's equation for a unit-strength point source located at $\mathbf{r} = \mathbf{r}_0$.) Let us for the moment impose no boundary conditions on $G(\mathbf{r},\mathbf{r}_0)$.

If we now let $\phi = U(\mathbf{r})$ and $\psi = G(\mathbf{r},\mathbf{r}_0)$ in Green's theorem (2.9) then we obtain

$$\begin{aligned}\int_V (U(\mathbf{r})\nabla^2 G(\mathbf{r},\mathbf{r}_0) - G(\mathbf{r},\mathbf{r}_0)\nabla^2 U(\mathbf{r}))\, dV(\mathbf{r}) \\ = \int_{\partial V}\left[U(\mathbf{r})\frac{\partial G(\mathbf{r},\mathbf{r}_0)}{\partial n} - G(\mathbf{r},\mathbf{r}_0)\frac{\partial U(\mathbf{r})}{\partial n}\right] d\left(\partial V(\mathbf{r})\right),\end{aligned} \tag{2.11}$$

where we made explicit that the volume and surface integrals are with respect to $\mathbf{r}$. Using

Equation (2.10) and Poisson's equation (2.8) the LHS can be simplified to give

$$\begin{aligned} 4\pi\gamma \int_V [U(\mathbf{r})\delta(\mathbf{r}-\mathbf{r}_0) - G(\mathbf{r},\mathbf{r}_0)\rho(\mathbf{r})]\, dV(\mathbf{r}) \\ = \int_{\partial V} \left[U(\mathbf{r}) \frac{\partial G(\mathbf{r},\mathbf{r}_0)}{\partial n} - G(\mathbf{r},\mathbf{r}_0) \frac{\partial U(\mathbf{r})}{\partial n} \right] \, d(\partial V\,(\mathbf{r}))\,. \end{aligned} \tag{2.12}$$

Since $\mathbf{r}_0$ lies within the volume V,

$$\int_V U(\mathbf{r})\delta(\mathbf{r}-\mathbf{r}_0)\, dV(\mathbf{r}) = U(\mathbf{r}_0), \tag{2.13}$$

and thus rearranging Equation (2.12) the solution to Poisson's equation (2.8) can be written

$$U(\mathbf{r}_0) = \int_V G(\mathbf{r},\mathbf{r}_0)\rho(\mathbf{r})\, dV(\mathbf{r}) + \frac{1}{4\pi\gamma} \int_{\partial V} \left[U(r) \frac{\partial G(\mathbf{r},\mathbf{r}_0)}{\partial n} - G(\mathbf{r},\mathbf{r}_0) \frac{\partial U(\mathbf{r})}{\partial n} \right] \, d\left(\partial V(\mathbf{r})\right). \tag{2.14}$$

Clearly, we can interchange the roles of r and r_0 in Equation (2.12) if we wish.

For the boundary conditions that we have imposed we require the solution for Poisson's equation (2.8) to take specific values on some surface ∂V that bounds V, that is we require that $U(\mathbf{r}) = 0$ on ∂V. This requirement causes the first term in the surface integral in Equation (2.14) to vanish.

Moreover, if we seek a Green's function $G(\mathbf{r},\mathbf{r}_0)$ for this problem it must clearly satisfy Equation (2.10), but we are free to choose the boundary conditions satisfied by $G(\mathbf{r},\mathbf{r}_0)$ in such a way as to make the solution (2.14) as simple as possible. From Equation (2.14), we see that by choosing

$$G(\mathbf{r},\mathbf{r}_0) = 0 \quad \text{for } \mathbf{r} \text{ on } \partial V \tag{2.15}$$

the second term in the surface integral vanishes too, and we have

$$\boxed{U(\mathbf{r}) = \int_V G(\mathbf{r},\mathbf{r}_0)\rho(\mathbf{r}_0)\, dV(\mathbf{r}_0)} \tag{2.16}$$

which is analogous to equation (2.4).

Thus for our boundary conditions we wish to find a Green's function that

1. satisfies Equation (2.10) and hence is singular at $\mathbf{r} = \mathbf{r}_0$, and

2. obeys the boundary condition $G(\mathbf{r},\mathbf{r}_0) = 0$ for $\mathbf{r}$ on ∂V.

Let us now solve Equation (2.10):

$$\frac{1}{4\pi\gamma}\nabla^2 G(\mathbf{r},\mathbf{r}_0) = \delta(r-r_0),$$

subject to the boundary condition: $G(\mathbf{r}, \mathbf{r}_0) \to 0$ as $|\mathbf{r}| \to \infty$. The physical content of this statement is clear: if one goes infinitely far from a point mass , its field dies off to zero. Since the problem is spherically symmetric about $\mathbf{r}_0$, let us consider a large sphere ∂V of radius R centered on $\mathbf{r}_0$, and integrate over the enclosed volume V. We then obtain

$$\frac{1}{4\pi\gamma}\int_V \nabla^2 G(\mathbf{r}, \mathbf{r}_0)\, dV(\mathbf{r}) = \int_V \delta(\mathbf{r} - \mathbf{r}_0)\, dV(\mathbf{r}) = 1, \tag{2.17}$$

since V encloses the point $\mathbf{r}_0$. However, using the divergence theorem

$$\int_V \nabla^2 G(\mathbf{r}, \mathbf{r}_0)\, dV(\mathbf{r}) = \int_{\partial V} \nabla G(\mathbf{r}, \mathbf{r}_0) \cdot \hat{\mathbf{n}}\, d(\partial V(\mathbf{r})), \tag{2.18}$$

where $\hat{\mathbf{n}}$ is the unit normal to the large sphere ∂V at any point. Since the problem is spherically symmetric about $\mathbf{r}_0$, we expect that

$$G(\mathbf{r}, \mathbf{r}_0) = G(\mathbf{r} - \mathbf{r}_0) = G(r), \tag{2.19}$$

i.e. G has the same value everywhere on ∂V. Thus, evaluating the surface integral in Equation (2.17), we have

$$\frac{r^2}{\gamma}\frac{dG}{dr}\bigg|_{r=R} = 1. \tag{2.20}$$

Integrating this expression we obtain

$$G(r) = \frac{-\gamma}{r} + \text{ constant} \tag{2.21}$$

but, since we require $G(\mathbf{r} - \mathbf{r}_0) \to 0$ as $|\mathbf{r}| \to \infty$, the constant must be zero. The fundamental solution in three dimensions is consequently given by

$$\boxed{G(\mathbf{r}, \mathbf{r}_0) = \frac{-\gamma}{|\mathbf{r} - \mathbf{r}_0|}.} \tag{2.22}$$

This is clearly also the full Green's function for Poisson's equation subject to the boundary condition $U(\mathbf{r}) \to 0$ as $|\mathbf{r}| \to \infty$.

3. The Gravity Gradient

The main aim of a geophysical survey is to collect geophysical data in order to determine the spatial distribution of materials in the earth. Geophysical surveys may use a great variety of sensing instruments, and data may be collected from above or below the Earth's surface or from aerial or marine platforms. In one type of measurement, a plane flies at nearly a constant height above the earth, which is an ellipsoid, with a special instrument called a *gradiometer* [Par90], which measures the gradient of the gravitational (force) field along the radial direction of the ellipsoid. Locally (that is, close to the earth's surface), we can approximate this radial direction with the vertical ($\hat{\mathbf{k}}$ in standard notation). In airborne surveys, the g_{zz} ($= \partial^2 U/\partial z^2$) component is usually measured because, as we will see in Section 3.2.2, it is that gradient component that is most sensitive to the surface geology. Gravity gradient data are measured in the units of Eötvos, with one Eötvos equal to $10^{-9}\,\mathrm{s}^{-2}$.

3.1 Vertical Gradient Fields

The gravitational force field, $\mathbf{g}$, is a conservative field and thus can be derived as the gradient of the gravitational potential:

$$\mathbf{g} = -\nabla U. \tag{3.1}$$

The gradiometer will measure

$$\frac{\partial}{\partial z}\,\hat{\mathbf{k}} \cdot \mathbf{g} = \frac{\partial}{\partial z} g_z \;\equiv\; -g_{zz} \;=\; -\frac{\partial^2 U}{\partial z^2}. \tag{3.2}$$

It is reasonable to assume that the gradiometer is always located at a source-free region (that is we will ignore the density of the surrounding atmosphere and the plane). Consequently the gravitational potential obeys Laplace's equation:

$$\nabla^2 U = 0 \tag{3.3}$$

If we restrict the gravitational potential to belong to a set of functions whose mixed partial derivatives up to and including fourth order are not singular, then we know that we can interchange the order of differentiation as is expressed by the following statement:

$$\left[\nabla \cdot \nabla, \frac{\partial^2}{\partial z^2}\right] = 0. \tag{3.4}$$

This in turn implies that g_{zz} is harmonic:

$$\nabla^2 g_{zz} = \nabla^2 \frac{\partial^2 U}{\partial z^2} \;=\; \frac{\partial^2}{\partial z^2} \nabla^2 U \;=\; 0. \tag{3.5}$$

Similarly,

$$\nabla^2 g_z = -\nabla^2 \frac{\partial U}{\partial z} \;=\; -\frac{\partial}{\partial z} \nabla^2 U \;=\; 0. \tag{3.6}$$

The harmonic nature of g_z and g_{zz} can possibly be expolited to remove noise from the measured signal.

Given the gravitational potential it is possible to define a second rank gradient tensor called the gravity gradient tensor, which is represented in matrix form below:

$$\mathcal{M} = \begin{pmatrix} \dfrac{\partial^2 U}{\partial x^2} & \dfrac{\partial^2 U}{\partial x \partial y} & \dfrac{\partial^2 U}{\partial x \partial z} \\ \dfrac{\partial^2 U}{\partial y \partial x} & \dfrac{\partial^2 U}{\partial y^2} & \dfrac{\partial^2 U}{\partial y \partial z} \\ \dfrac{\partial^2 U}{\partial z \partial x} & \dfrac{\partial^2 U}{\partial z \partial y} & \dfrac{\partial^2 U}{\partial z^2} \end{pmatrix}.$$

With a complete knowledge of this gradient tensor, it is possible to reconstruct both the gravitational field and the gravitational potential. There will be an arbitrary constant that will enter into the expression for the gravitational field obtained by integrating the gradient tensor. This arbitrary constant is determined by specifying the value of the gravitational field at a single (known) position. There will also be an arbitrary constant of integration entering into the expression for the gravitational potential obtained by integrating the gravitational field – this constant cannot be determined and simply represents the usual arbitrariness in defining a potential.

It is not quite necessary to have a complete knowledge of the gradient tensor, since in general, not all components of the tensor are independent. One can argue that there are five independent components in the gradient tensor, by noting that (i) equality of mixed partial derivatives implies that $\mathcal{M}$ is symmetric and (ii) Laplace's equation implies that $\mathcal{M}$ is traceless.

Since g_{zz} is the only component of the gradient tensor which is measured, four independent components have been dropped. In the following paragraphs we argue that for a suitable choice of boundary conditions we do not need the other components of the gravity tensor to determine the gravitational field and the gravitational potential.

Integrating both sides of

$$-\frac{\partial U}{\partial z} = g_z, \tag{3.7}$$

we have

$$\int_{U(x,y,z)}^{U(x,y,\infty)} dU = U(x,y,\infty) - U(x,y,z) = -\int_z^\infty g_z(x,y,z')\,dz'. \tag{3.8}$$

Although we do not have knowledge of the detailed structure of the source, we certainly do know that it can't continue indefinitely above the plane $z = 0$. Thus it is reasonable to require $U \to 0$ as $z \to \infty$, i.e., $U(x,y,\infty) = 0$, and Equation (3.8) becomes

$$U(x,y,z) = \int_z^\infty g_z(x,y,z')\,dz'. \tag{3.9}$$

Similarly, by taking $g_z(x,y,\infty) = 0$, we have

$$g_z(x,y,z) = \int_z^\infty g_{zz}(x,y,z')\,dz'. \tag{3.10}$$

The inverson of potential fields (i.e., the determination of the density distribution from potential field measurements) is not well defined – there are always ambiguities in reconstructing the sources from a given set of measurements of the potential, taken in a source free region. The ambiguities cannot be resolved using purely mathematical arguments – intuitively we may say something like a very massive but distant source gives rise to the same field as a less massive but nearby source. We will refer to these arbiguities as source ambiguities. The result obtained is completely unrelated to source ambiguities. What we are saying is that the potential can be determined uniquely at the flying height of the aircraft given

1. The fact that the acceleration g_z drops off to to zero as z increases to infinity
2. The potential U goes to a constant as z increases to infinity and
3. An exact value of the gradient for all $|z| \geqslant 0$.

Even if we have the exact potential at the flight height, we are still no closer to resolving the source ambiguities inherent in the problem.

3.2 The Digital Terrain Model

When the gravity survey is completed, now comes the interesting challenge of interpretation. The problem is conceptually straightforward: estimate one or more parameters of the source from observed gravity fields, while incorporating all available geologic, geophysical, and other independent information.

The many techniques of interpretation can be divided into three categories [Bla96]:

1. *Forward method*: An initial model (for example the **digital terrain model** (**DTM**) which is a digital representation of ground surface topography or terrain) for the source body is constructed based on geologic and and geophysical intuition. Values for the model's gravitational field (including the gravity gradient) are calculated and compared with the observed values, and model parameters are adjusted in order to improve the fit between the two sets of values. This three-step process of body adjustment, calculation, and comparison is repeated until calculated and observed values are deemed sufficiently alike.
2. *Inverse method*: One or more body parameters are calculated automatically and directly from the observed data. Simplifying assumptions are inevitable.
3. *Data enhancement and display*: No model parameters are calculated per se , but the data is processed in some way in order to enhance certain characteristics of the source, thereby facilitating the overall interpretation.

3.2.1 The Dipole Effective Model

In this section, we limit ourselves to the forward model which will be used to determine g_z and g_{zz}. The forward model of the gravity problem involves convolving Green's function with the source of the field (see Equation (2.16)), that is, with the digital terrian model. The forward model will be used to determine the gravitational gradients along the vertical axis z. In this section we will focus on the case that one has a constant density terrian correction in mind and simply point out what modifications arise from a non-constant terrain density. The forward model to obtain g_z is given by

$$g_z(\mathbf{r}) = -\frac{\partial U}{\partial z} \;=\; -\int_{\mathsf{DTM}} \frac{\partial G(\mathbf{r}-\mathbf{r}')}{\partial z}\rho\, d^3r', \tag{3.11}$$

where $G(\mathbf{r}-\mathbf{r}') = -\gamma/|\mathbf{r}-\mathbf{r}'|$ is Green's funtion for the gravitational potential (see Equation (2.22)).

The calculation of the vertical gravity gradient response can similarly be obtained by differentiating the g_z component with respect to z . That is

$$g_{zz}(\mathbf{r}) = \frac{\partial g_z}{\partial z} \;=\; \int_{\mathsf{DTM}} \frac{\partial^2}{\partial z^2} G(\mathbf{r}-\mathbf{r}')\rho\, d^3r' \tag{3.12}$$

Note that $\partial^2 G(\mathbf{r}-\mathbf{r}')/\partial z^2 = \partial^2 G(\mathbf{r}-\mathbf{r}')/\partial z'^2$, thus it is now possible to integrate by parts with respect to z'. The fact that we are performing a constant density correction implies that the bulk term (which contains $\partial\rho/\partial z$)) vanishes. The advantage of performing this integration by parts is that we are left with equations that involve the Green's function for gravity g_z. Then we can compare the sources appearing in the once-integrated-by-parts equation with the sources appearing in the gravity equations. Neglecting the bulk term, forward model will reduce to evaluating the integral

$$g_{zz}(\mathbf{r}) = \int_{\partial(\mathsf{DTM})} \left[\frac{\partial G(\mathbf{r}-\mathbf{r}')}{\partial z}\rho\right]_{z'=z_-(x',y')}^{z'=z_+(x',y')} dx'\, dy'. \tag{3.13}$$

over the surface of the digital terrain model. The function $z_+(x,y)$ is the upper z coordinate of the terrain at the point (x,y) and the function $z_-(x,y)$ is the lower z coordinate of the terrain at the point (x,y). We can alternatively express Equation (3.13) in vector form using elements $d\mathbf{A}'$ of the DTM surface area directed normal to the surface and pointing outwards. The integrand also has to be assigned a direction, which can be acheived with the help of a unit vector $\hat{\mathbf{s}}(\mathbf{r})$.

$$g_{zz}(\mathbf{r}) = \int_{\partial(\mathsf{DTM})} \frac{\partial G(\mathbf{r}-\mathbf{r}')}{\partial z}\rho\hat{\mathbf{s}}(\mathbf{r})\cdot d\mathbf{A}'. \tag{3.14}$$

The vector $\hat{\mathbf{s}}$ is assigned a direction such that it makes an angle θ with $d\mathbf{A}'$ and so that

$$\cos\theta(\mathbf{r}') = \frac{dx'dy'}{dA} \tag{3.15}$$

where $dA = \sqrt{d\mathbf{A}\cdot d\mathbf{A}}$.

The above expression has been written in such a way that the source $\rho\hat{\mathbf{s}}(\mathbf{r})$ looks like a vector. In addition, the Green's function used to compute the response *is the Green's function usually used to compute the g_z response*. Thus the above expression models the gravity gradient response as the response from an effective source of "gravity dipoles" on the surface of the digital terrain model, hence the name **Dipole Effective Model**.

To summarize, instead of breaking the bulk of the digital terrain model up into a collection of monopole gradient sources, the surface of the digital terrain model can be decomposed into a collection of "gravity dipole" sources.

Now let us consider the situation in which the density distribution is no longer constant in the terrain model. There is an extra bulk contribution

$$-\int_{\text{DTM}} \frac{\partial G(\mathbf{r}-\mathbf{r}')}{\partial z}\,\frac{\partial \rho(\mathbf{r}')}{\partial z'}\,d^3r'. \tag{3.16}$$

Thus when the terrain density is not constant one has an effective source which has both a gravity "vector" $\hat{\mathbf{s}}(\mathbf{r})$ and a gravity "scalar" $\frac{\partial \rho}{\partial z}$ contribution.

3.2.2 Spatial Dependence of Green's Function

Green's functions for the gradient field contain information on how the gradient field scales with distance or position. The gravitational potential at a location $\mathbf{r}$ due to unit point source at the origin is given by Green's function for the gravitational potential:

$$G(\mathbf{r}) = -\frac{\gamma}{r}, \tag{3.17}$$

where $r = |\mathbf{r}| = \sqrt{x^2+y^2+z^2}$. In computing the Green's function for the gravity gradient, we differentiate (twice) the potential due to the point source (see Equation (3.12)). The Green's function for the vertical gradient is

$$g_{zz} = \frac{\partial^2 G(\mathbf{r})}{\partial z^2} \;=\; -\frac{\gamma}{r^3}\frac{(3z^2-r^2)}{r^2}. \tag{3.18}$$

Similarly we can compute the other components of the Green's function for the gravity gradient giving

$$g_{xx} = -\frac{\gamma}{r^3}\frac{(3x^2-r^2)}{r^2}; \quad g_{yy} \;=\; -\frac{\gamma}{r^3}\frac{(3y^2-r^2)}{r^2} \tag{3.19}$$

$$g_{xy} = -\frac{\gamma}{r^3}\frac{3xy}{r^2}; \quad g_{yz} \;=\; -\frac{\gamma}{r^3}\frac{3yz}{r^2}; \quad g_{xz} \;=\; -\frac{\gamma}{r^3}\frac{3xz}{r^2} \tag{3.20}$$

Plots of these components on the $z = 1$ plane are shown below in Figures (3.1) to (3.6).

The Green's functions measure the response from a point source. Points of equal height on the surface (of the plot) can be interpreted as points of equal sensitivity. For g_{zz} which is of most interest, the instrument sensitivity peaks when it is directly over the point source, where it has a large and narrow lobe. The sensitivity rapidly drops to zero as one moves away from the point source (see Figure (3.3)). The difference between the maximum and minimum values of the response is greatest for the g_{zz} component of the gravity gradient tensor. Also note that the gravity gradient tensor has a "circle of zeros" at $r^2 = 3z^2$.

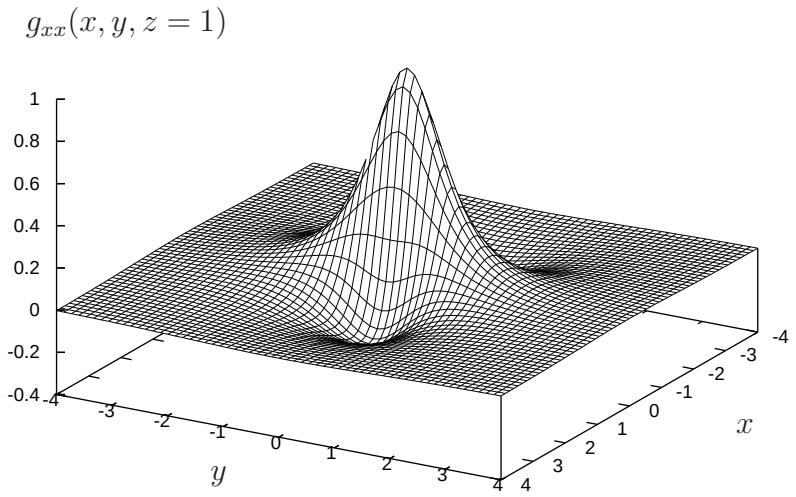

Figure 3.1: The g_{xx} response to a unit point source at the origin. The response is calculated on the $z = 1$ plane. The response is measured in units of γ.

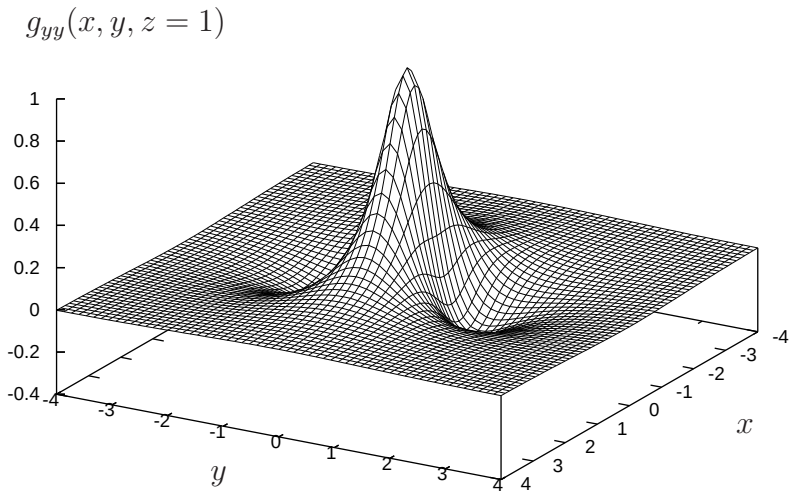

Figure 3.2: The g_{yy} response to a unit point source at the origin. The response is calculated on the $z = 1$ plane. The response is measured in units of γ.

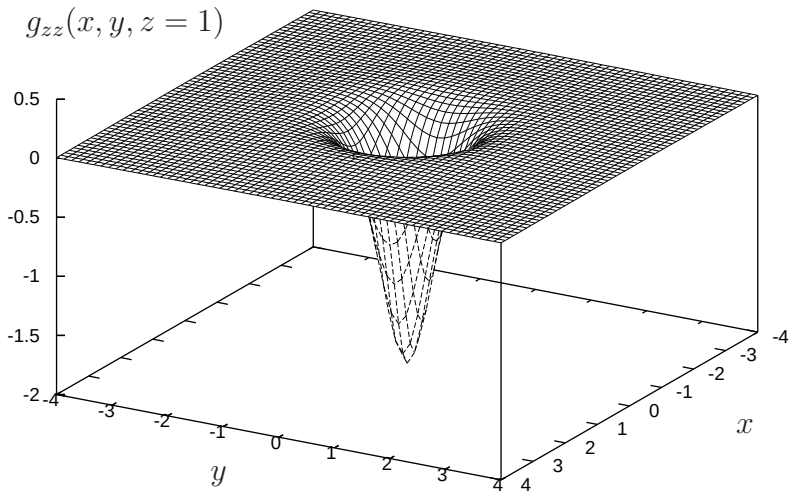

Figure 3.3: The g_{zz} response to a unit point source at the origin. The response is calculated on the $z = 1$ plane. The response is measured in units of γ.

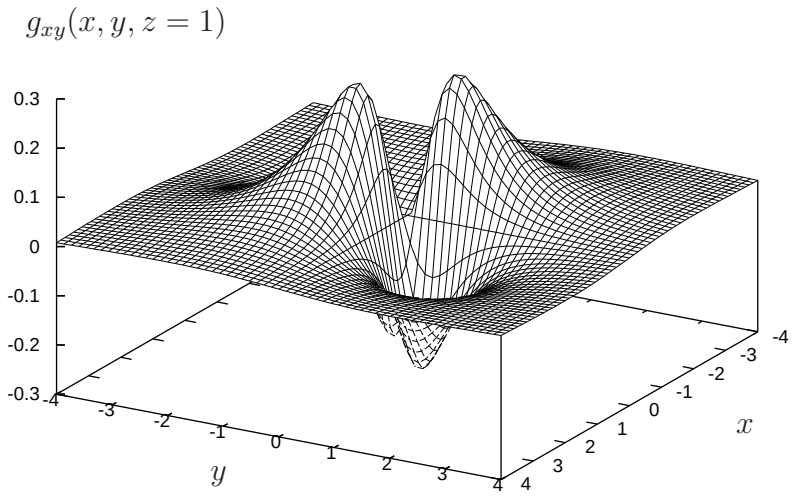

Figure 3.4: The g_{xy} response to a unit point source at the origin. The response is calculated on the $z = 1$ plane. The response is measured in units of γ.

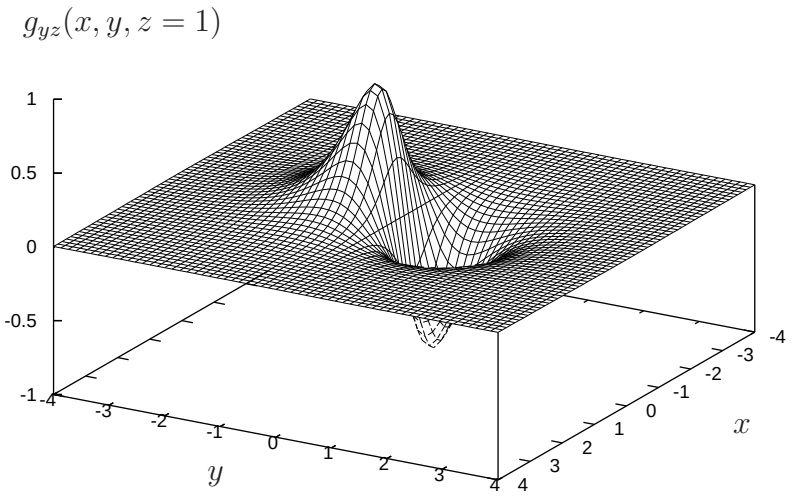

Figure 3.5: The g_{yz} response to a unit point source at the origin. The response is calculated on the $z = 1$ plane. The response is measured in units of γ.

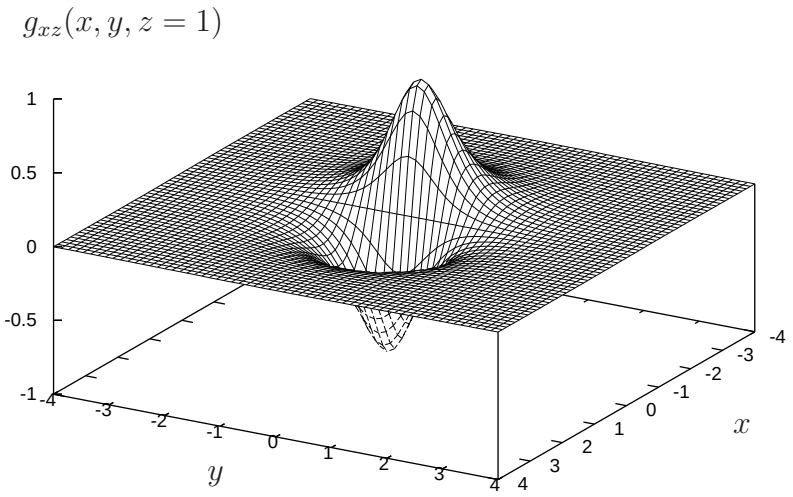

Figure 3.6: The g_{xz} response to a unit point source at the origin. The response is calculated on the $z = 1$ plane. The response is measured in units of γ.

4. Correction of Gradients

4.1 Observed Gravity

In this section, we are going to decompose the observed gravity (gradient) measured in a gravity survey. Initially we show that the gradient measured at the surface or beneath the earth is subject to variations which reflect in the variation of density and crustal materials of the earth. The contributing factors that result in the decomposition of the observed gravity measurements are as follows [Bla96]:

$$\begin{aligned} \text{Observed gravity} &= \text{Theoretical Gravity (gradient)} \\ &+ \text{Free Air Correction} \\ &+ \text{Bouguer correction} \\ &+ \text{Time Dependent Tidal Variation} \\ &+ \text{Eötvös correction} \\ &+ \text{Isostatic Correction} \\ &+ \text{Measurement Noise} \\ &+ \text{anomalies.} \end{aligned}$$

An *anomaly* is the difference between the observed gravity and the correction due to any of the contributing factors of the gravity reading. These corrections can be modelled accurately and reliably, with the possible exception of measurement noise. Each contributing term in the observed gravity will be discussed and will lead us to coding the results that will be amenable to computer.

4.1.1 Theoretical Gravity

As a first approximation, one can assume that the earth is a perfect ellipsoid. Thus, the surface of the earth (sea level) would be an equipotential. This equipotential is usually called the *geoid*, and the value of the gravitational field as computed from the geoid is called *theoretical gravity*. Similarly, the value of g_{zz} computed from the geoid will be called *theoretical gradient*. The theoretical gravity is computed from the geoid. The so-called Somigiliana equation is used to compute the geoid and is given as [Bla96]

$$g_0 = g_e \frac{1 + k \sin^2 \lambda}{\sqrt{1 - e^2 \sin^2 \lambda}} \tag{4.1}$$

where g_0 the gravitational attraction of the reference ellipsoid at any point, λ is the latitude, and the constants g_e, k, and e depend on the angular velocity (ω) of the mass M, the flattening parameter f, and equatorial radius (a) of the earth. This geoid has been measured by the

International Association of Geodesy (1984), using data taken by satellites. The values of the parameters of the geoid are given in the formula below [Bla96]:

$$g_0 = 9.7803267714 \frac{1 + 0.00193185138513639 \sin^2(\lambda)}{\sqrt{1 - 0.000669437999013 \sin^2(\lambda)}}. \tag{4.2}$$

This formula for g_0 is measured in m/s^2. By taking derivative of the Somigliana equation and evaluating the resulting expression gives [Bla96]

$$g_{zz} = \frac{\partial g_0}{\partial z} = -2g_0\kappa - 2\omega^2. \tag{4.3}$$

for the value of the gradient of the gravitational attraction of the reference ellipsoid. This formula is known as Bruns' formula. The parameter κ, the mean curvature of the ellipsoid, is given by

$$\kappa = \frac{1}{2}\left(\frac{1}{M} + \frac{1}{N}\right) \tag{4.4}$$

where M and N are the principal radii of curvature. Using the values given in World Geodetic System (1984), one obtains that

$$g_{zz} = 3086\text{Eö} \quad \text{[World Geodetic 1984]}.$$

4.1.2 Free Air Correction

Gravity measurements are made on the reference geoid. To calculate the free air correction one needs to add a term to the theoretical gravity which accounts for the elevation above or below sea level.

Before computing the correction to the gradient, the correction to the gravitational field will be reviewed and well established. The correction to the gravitational gradient can also be performed in the same way, so that reviewing of the gravitational field is a helpful exercise. The value of the gradient of the gravitational potential at a distance h above the geoid is

$$\frac{\partial U(r+h)}{\partial z} = \frac{\partial U(r)}{\partial z} + h\frac{\partial^2 U(r)}{\partial z^2} + \frac{h^2}{2!}\frac{\partial^3 U(r)}{\partial z^3} + \dots. \tag{4.5}$$

Rearranging the terms in equation 4.5 and solving for the gravitational field, we can deduce that

$$g_z(r) = \frac{\partial U(r)}{\partial z} = \frac{\partial U(r+h)}{\partial z} - h\frac{\partial^2 U(r)}{\partial z^2} - \frac{h^2}{2!}\frac{\partial^3 U(r)}{\partial z^3} - \dots. \tag{4.6}$$

In equation 4.6 the higher order terms of h are dropped since measurements are taken sufficiently close to the surface of the earth. Substituting for the value of the radius of the earth and the value for gravity at sea level, we are able to calculate the gravitational field at any finite height from the surface of the earth. In general we can express the gravitational attraction as

$$h\frac{\partial^2 U(r)}{\partial z^2} = 0.3086 \times 10^{-5} h. \tag{4.7}$$

The free air correction is necessary because it is the only elevation adjustment required if no masses were to exist between the observation point and sea level. If we measure h in centimeters,the above free air anomaly is also measured in $Gals$. If we measure h in SI units the free air gradient correction will be in $\mathrm{m} \cdot \mathrm{sec}^{-2}$. Recall that h is the height above sea level and is the difference in elevation between $g(r)$ and $g(r+h)$. Application of the free air correction provides the free air anomaly given by [Bla96]

$$\Delta g_{fa} = g_{obs} - g_{fa} - g_0, \tag{4.8}$$

where g_{obs} is the observed gravity.

Over elevated areas of land, the free air anomaly tends to rise to large values, which causes an often undesirable correlation between topography and gravity. Since the free air correction does not account for the mass, an increase height of a gradiometer above the earth also account for a large increase anomaly. Nevertheless, the free air anomalies are often used in geodesy for the studies of the spheroid because they are very nearly equivalent to what would be observed if the topographic masses were condensed onto the geoid.

The computation for the free air correction to the gradient measurement is performed in exactly the same way. The gradient of the field at distance h above the geoid, is given by

$$\frac{\partial^2 U(r+h)}{\partial z^2} = \frac{\partial^2 U(r)}{\partial z^2} + h\frac{\partial^3 U(r)}{\partial z^3} + \frac{h^2}{2!}\frac{\partial^4 U(r)}{\partial z^4} + \dots. \tag{4.9}$$

Rearranging, we find

$$g_{zz}(r) = \frac{\partial^2 U(r)}{\partial z^2} = \frac{\partial^2 U(r+h)}{\partial z^2} - h\frac{\partial^3 U(r)}{\partial z^3} - \frac{h^2}{2!}\frac{\partial^4 U(r)}{\partial z^4} + \dots. \tag{4.10}$$

Dropping any higher order terms the vertical gradient can be calculated as

$$h\frac{\partial^3 U(r)}{\partial z^3} = 4.855 \times 10^{-4} h \tag{4.11}$$

The unit of the above correction is Eö when h is measured in meters above sea level.

4.1.3 Tidal Correction

Gravity measured at a fixed location varies with time because of periodic variation in the gravitational effects of the sun and the moon associated with their orbital motions. These combined effects are referred to as tidal variations. The application of tidal correction is not necessary in this report, since we are interested in the gradient measurement. The tidal effect occurs periodically every 12 hours. Tidal corrections are effects from distant sources. Since the gradient falls off as r^{-3} (as opposed to r^{-2} for the field and r^{-1} for the potential), sources that are distant can be neglected. The theoretical model for tidal corrections to gradient measurements is not included in this report. If these corrections are not negligible, they will need to be taken into account in the process of levelling the data. In this context they will naturally be modelled as a source of instrument drift.

4.1.4 Eötvös Correction

The gravitational attraction at a point fixed with respect to the earth is reduced by the centrifugal force related to the earth's rotation. The angular velocity of an observer moving east is greater than for a stationary observer, consequently the gravitational attraction for the moving observer is slightly reduced. Likewise, gravitational attraction will be slightly increased for an observer moving in a Westerly direction. This coupling between the aircraft's velocity and the earth rotation is called the Eötvös effect. The Eötvös effect on gravity measurement is accounted for in moving platforms such as in aircraft and ships. The effect is most easily accounted for by introducing a rotational potential [Wil02]

$$U_r = \frac{1}{2}\omega^2 r^2 \cos^2 \lambda, \tag{4.12}$$

where λ is the latitude, ω is the angular velocity measured (in rad/s) and r is the radius of the earth. The Eötvös correction is now easily derived from this potential as

$$g_{Evs} = 2v_e\omega \cos\phi + \frac{v_n^2}{a}\left(1 + \frac{h}{a} + e(2 - 3\sin^2\phi)\right) + \frac{v_e^2}{a}\left(1 + \frac{h}{a} - e\sin^2\phi\right), \tag{4.13}$$

where v_n is the component of the platform velocity (in 10^{-5} cm/s in the Northerly direction, V_e is the component of the platform velocity (in 10^{-5} cm/s) in the Easterly direction, ω is the earth's rotation rate(in rad/sec), ϕ is the latitude in degrees, h is the height (in cm) of the aircraft above the geoid, e is the earth flattening for the reference ellipsoid, a is semi-major radius (in cm) and g_{Evs} is measured in mGal.

The gradiometer mounted on an aircraft measures the vertical gradient of the gravitational field due to the anomalous masses, but the noise arises because the aircraft is not an inertial reference frame which we need to take into account in its motion. More worying is that the vertical accelerations of the aircraft respond to wavelengths that closely correspond to topographic features. This implies that this particular noise cannot be removed by low pass filtering the data. Since the origin of this noise is linked to the motion of the aircraft, it cannot be modelled accurately and it is therefore not a trivial task to remove this noise.

The vertical gradient of the g_{Evs} is

$$\frac{\partial g_{Evs}}{\partial z} = \frac{v_e^2 + v_n^2}{a^2}. \tag{4.14}$$

In writing this formula, we have used the fact that

$$\frac{\partial h}{\partial z} = 1, \tag{4.15}$$

and we have assumed that v_e and v_n do not depend on z. It is reasonable to approximate the speed of the aircraft as 283km/hr at the height of 100m, then

$$\frac{\partial g_{evs}}{\partial z} = 0.15\text{Eö}. \tag{4.16}$$

The unit for the above Eötvös gradient correction is Eö. Thus, the Eötvös correction to the gradient data can be neglected. This is intuitively pleasing. If one considers an instrument moving on a perfect path of radius r, the centrifugal force falls off as r^{-2}. The gradient of the centrifugal force falls off rapidly as r^{-3}. This fast fall with radial distance responsible for removing the free air and tidal corrections, is also the mechanism which removes the Eötvös correction.

4.1.5 Bouguer Correction

The free air correction and theoretical gravity ignore mass that may exist between the level of observation and sea level. The simple Bouguer correction approximates all mass above sea level with a homogeneous, infinitely extended slab of thickness equal to the height of the observation point above sea level. Considering that the thickness is h and is constant at a particular point, the gravitational attraction observed is

$$g_{sb} = 2\pi\gamma\rho h\hat{\mathbf{k}}. \tag{4.17}$$

Substituting for the typical crustal density ($\rho = 2670kg \cdot m^{-3}$) the simple Bouguer correction becomes

$$g_{sb} = 0.1119 \times 10^{-5}h. \tag{4.18}$$

Ignoring the tidal and Eötvös corrections the simple Bouguer correction is expressed as

$$\Delta g_{sb} = g_{obs} - g_{fa} - g_{sb} - g_0. \tag{4.19}$$

The above expression ignores the shape of topography features. Valleys and mountains that rise above the observation level "pull up" on gravity meter but are not accounted for in the slab approximation. In such conditions the simple Bouguer correction overcompensates measurement made near topographic features. The terrain correction ($\mathbf{g}_t$) adjust this overcompensation and the complete Bouguer correction is then expressed as

$$\Delta g_{sb} = g_{obs} - g_{fa} - g_{sb} - g_t - g_0, \tag{4.20}$$

where the sign of g_t is always negative.

Apart from the slab model the complete Bouguer correction accounts for the Terrain correction which takes into account the curvature of the earth [Bla96] and is traditionally done by the approximating the topography with the digital terrain model. LaFehr [Bla96] computed this model by assuming that the earth is spherical and the curvature correction can be taken care of by measuring the spherical cap. See Figure (4.1) below.

The spherical cap does two things to the Bouguer anomaly:

1. it truncates the portion of the slab coloured grey in the above diagram, and
2. it adds the (nearly triangular in cross section) ring coloured black in the above diagram.

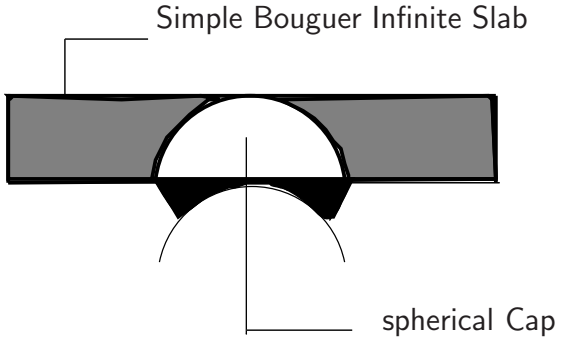

Figure 4.1: Cross section of Sperical cap.

The cap of the spheroid of thickness h should correspond to the arc length of at least 167.7km on the surface of the earth that has been truncated to an angle of β the zone of truncation is referred to as the Hayford-Bowie zone O. Taking a sector to model, we can let R_0 be the radius of the slab at the bottom and $R = h + R_0$ be the radius of the slab at the top. To determine the curvature correction, one needs to compute the attraction of the spherical cap of the region A as shown in Figure (4.2) below.

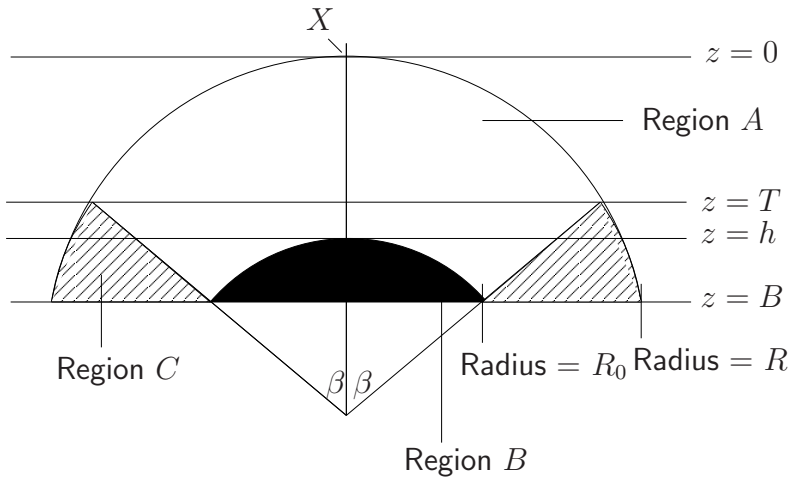

Figure 4.2: To compute the gravitational attraction of the spherical cap (shown as region A in the figure) it is easiest to compute the gravitational attraction for the sum of regions A, B, and C, and then to subtract the attractions from regions B and C

.

The attraction of the spherical cap will be computed by first computing the attraction from the sum of the region marked A, B and C) and then subtracting the attraction from region mark B

and C. The integrals to compute in this case are

$$\begin{aligned} I = \gamma\rho \int_{A+B+C} \left(\frac{3z^2}{(x^2+y^2+z^2)^{5/2}} - \frac{1}{(x^2+y^2+z^2)^{3/2}} \right) dxdydz \\ - \gamma\rho \int_{B} \left(\frac{3z^2}{(x^2+y^2+z^2)^{5/2}} - \frac{1}{(x^2+y^2+z^2)^{3/2}} \right) dxdydz \\ - \gamma\rho \int_{c} \left(\frac{3z^2}{(x^2+y^2+z^2)^{5/2}} - \frac{1}{(x^2+y^2+z^2)^{3/2}} \right) dxdydz. \end{aligned} \tag{4.21}$$

The result of this integral is the value of the gravitational gradient at the point marked X in the diagram of the spherical cap. The integration region and integrand are both invariant under rotations in the $x-y$ plane. For this reason, it is convenient to change to new variable -an angle and a radius. The integral over the angle is trivial and leads to

$$\begin{aligned} I = -2\pi\gamma\rho \int_0^{\sqrt{R^2-(R-z)2}} dr \int_0^B \left(\frac{3z^2 r}{(r^2+z^2)^{5/2}} - \frac{r}{(r^2+z^2)^{3/2}} \right) dz \\ + 2\pi\gamma\rho \int_0^{\sqrt{R^2-(R-z)^2}} dr \int_h^B \left(\frac{3z^2 r}{(r^2+z^2)^{5/2}} - \frac{r}{(r^2+z^2)^{3/2}} \right) dz \\ + 2\pi\gamma\rho \int_{\sqrt{(R-z)^2\tan^2\beta}}^{\sqrt{R^2-(R-z)^2}} \int_T^B \left(\frac{3z^2 r}{(r^2+z^2)^{5/2}} - \frac{r}{(r^2+z^2)^{3/2}} \right) dz \end{aligned} \tag{4.22}$$

integrating over r yields the follows.

$$\begin{aligned} I = 2\pi\gamma\rho \int_0^B \left(\frac{3z^2 r}{(r^2+z^2)^{5/2}} - \frac{r}{(r^2 z^2)^{3/2}} \right)_0^{\sqrt{R^2-(R-z)^2}} dz \\ - 2\pi\gamma\rho \int_h^B \left(\frac{3z^2 r}{(r^2+z^2)^{5/2}} - \frac{r}{(r^2 z^2)^{3/2}} \right)_0^{\sqrt{R^2-(R-z)^2}} dz \\ - 2\pi\gamma\rho \int_T^B \left(\frac{3z^2 r}{(r^2+z^2)^{5/2}} - \frac{r}{(r^2+z^2)^{3/2}} \right)_{\sqrt{(R-z)^2\tan^2\beta}}^{\sqrt{R^2-(R-z)^2}} dz \end{aligned} \tag{4.23}$$

After the final integration over z we have

$$\begin{aligned} I = 2\pi\gamma\rho \left[\frac{2}{3} \left(\frac{z}{2R} \right)^{2/3} - 2\sqrt{\frac{z}{2R}} \right]_0^B - 2\pi\gamma\rho \left[\frac{2}{3} \left(\frac{z}{2R_0} \right)^{2/3} - 2\sqrt{\frac{z}{2R_0}} \right]_h^B \\ - 2\pi\gamma\rho \left[- \left(\frac{(1-\tan^2\beta)z + R\tan^2\beta}{(1+\tan^2\beta)\sqrt{z^2+(R-z)^2\tan^2\beta}} \right) - \frac{2}{3} \left(\frac{z}{2R} \right)^{2/3} - 2\sqrt{\frac{z}{2R}} \right. \\ - \frac{\tan^2\beta}{(1+\tan^2\beta)^{3/2}} \log \left(2\sqrt{1+\tan^2\beta}\sqrt{z^2+(R-z)^2\tan^2\beta} + 2(1+\tan^2\beta)z \right. \\ \left. \left. -2R\tan^2\beta \right) \right]_T^B. \end{aligned} \tag{4.24}$$

The parameter appearing in this expression obeys the following relations

$$T = R - R\cos\beta, \quad B = R_0\cos\beta, \quad \beta = \frac{s}{R_0}$$

with the S equal to the arc length traced out by β, measured along the Earth's surface. We take the length S to be 166.7km which corresponds to the Hayford-Bowie zone O. To calculate for the curvature we substitute for the value of $2\pi\gamma\rho = 0.1119 \times 10^{-5}$ in the above formula and compute some hypothetical corrections for some height. A few results are shown in the table below.

h(m)	100m	500m	1000m	2500m	5000m
I(Eö)	4. 86	6. 68	5. 33	-3. 28	-21. 08

It is interesting to note that LaFehr obtains a maximum value for g_z sourced by the cap at $\simeq 2km$. Our result has a zero at this point, as expected. Although these corrections may in fact be larger then the noise levels that can be tolerated, this correction will be a (nearly) constant offset for all the gradient readings in the survey area and consequently will automatically be removed taking measurements relative to a fixed base value.

4.1.6 Isostatic Residual

Continents and ocean basins represent mass concentrations and deficiencies, respectively, with large lateral dimensions; it seems that such profound masses should be reflected in low-order harmonic terms of the geoid. This is not the case, however, as can be seen from global scale maps of the geoid. Apparently, large mass concentrations and mass deficiencies are compansated at depth, so that total mass in each vertical section is laterally uniform to first order [Bla96]. The phenomenon of compensation of topographic loads by deeper compensating masses is referred to as *isotatic compensation*

The isostatic residual correction involves subtracting the anomaly caused by these compensating masses. These anomalies are of the order of $mGal$ and must be accounted for in gravity measurements.

According to the Airy model of isotatic compensation, the total mass must be equal for all columns extending from the earth's surface to some depth of compensation[Bla96] (see Figure (4.3) below).

In the Figure (4.3) the mass in Column 1 is proportional to $d_s\rho_c + (d_m - d_s)\rho_m$, where d_s is the depth of compensation at the shorelines, d_m is the depth below sea level of the compensating root, ρ_c is the crustal density, and ρ_m is mantle density. The mass in Column 2 is proportional to $h\rho_t + d_m\rho_c$, where ρ_t is the average density of rocks that make up the terrian, and h is the elevation of the observation point above sea level. Equating the two mass columns provides [Bla96]

$$d_m = h\frac{\rho_t}{\Delta\rho} + d_s \ , \tag{4.25}$$

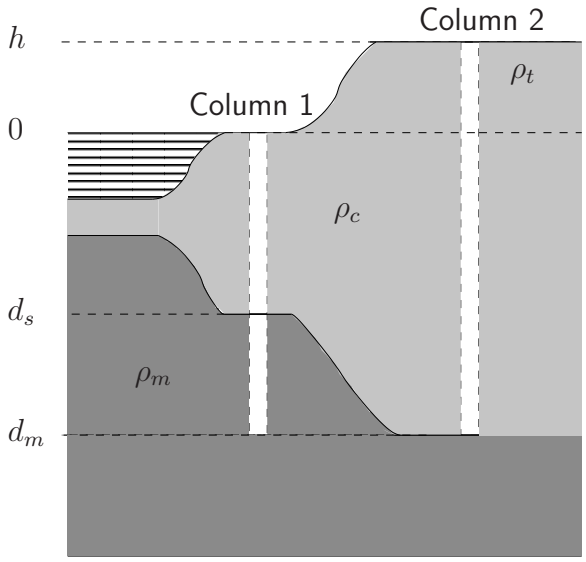

Figure 4.3: Two crustal comlumns of equal total mass in an Airy model of isostatic compensation.

where $\Delta\rho = \rho_m - \rho_c$. Note that the depth to the root depends on the contrast across the crust-mantle interface, not on the absolute values of ρ_c and ρ_m.

The gravitational effect of any terrain can be calculated by using the digital terrain model. To calculate the isotatic correction we substract the isostatic regional anomaly g_{i} which will result in the isostatic residual anomaly

$$\Delta g_{\text{i}} = g_{obs} - g_{fa} - g_{sb} - g_t - g_{\text{i}} - g_0. \tag{4.26}$$

The isostatic regional anomaly is negative over continents and positive over oceans. In most geophysical surveys the depth of compensating masses are generally greater then 20km which is roughly the same size as the earth's crust. Thus the large depth of compensating masses suggests that the r^{-3} fall-off of the gradient will suppress the isostatic residual correction. For example let us consider a mass with density 0.3g/cm^3 in the earth crust and of dimensions $50\text{km} \times 50\text{km} \times 5\text{km}$. The mass excess is compensated by a mass deficiency at depth of 25km, with dimensions of $50\text{km} \times 50\text{km} \times 3.750\text{km}$ and density of -0.4g/cm^3. Below we have computed the attraction of the crustal mass and the compensating root. Also shown in Figure (4.4) is the gradient due to the dense crustal mass and the gradient of the compensating root. see diagram.

The gradient sourced by the root indicates the size of the isostatic correction. From the graph above, the local Airy-Heiskanen root makes a contribution as high as 5.59 E$\ddot{0}$ [Bla96]. In a high precision survey this anomaly will have to be accounted for. This correction will be more important if the scale of the survey is large.

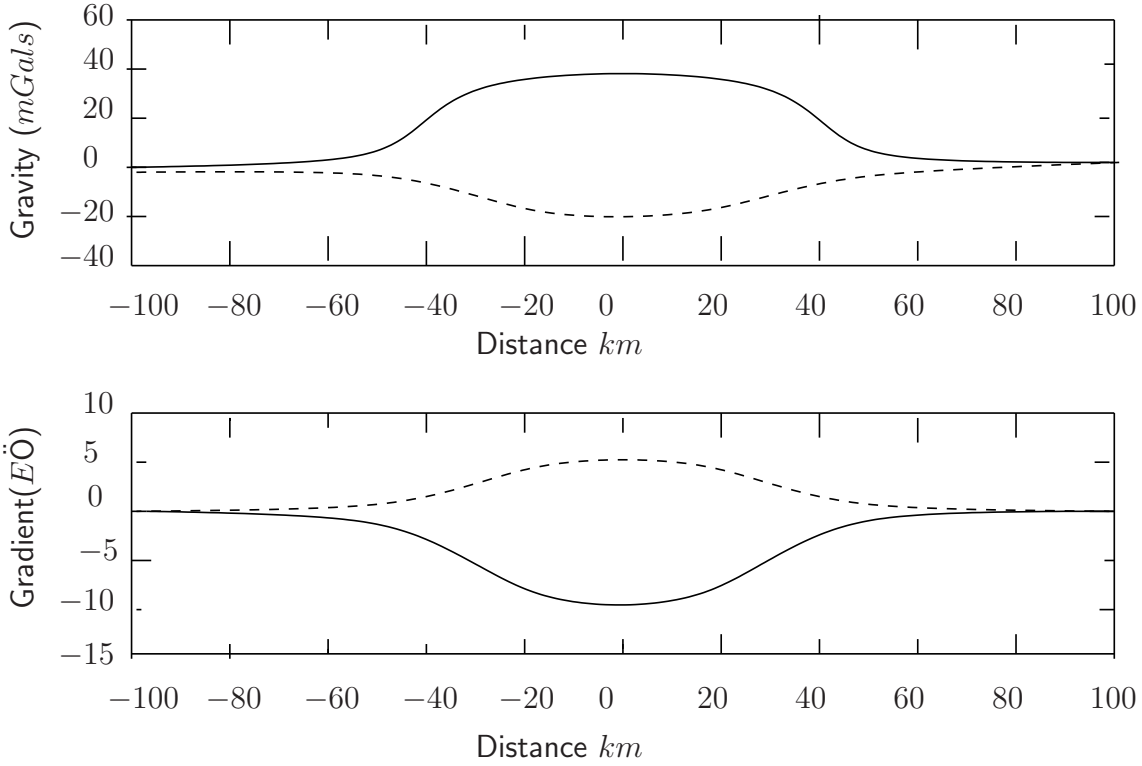

Figure 4.4: The attractions and gradients due to crustal mass and the compensating root. The crustal mass is plotted with a solid line, the root with a dashed line.[dMKP01]

4.2 New Sources of Error

In our previous discussion we observed that the majority of the effects accounted for in reducing the gravitional field, do not play a significant role in reduction of the gradient field. This suggests the logical possibility that new corrections that are not important in gravity measurements will have to be accounted for when dealing with the gradients. This is almost certainly the case. We mentioned in Section 3.2 that the source of the gradient field can be taken as a collection of the gravity dipole sources, distributed on the surface of the digital terrain model. A crucial difference between a monopole and dipole source is that the dipole source has a definite orientation. Clearly then, errors in the elevation measurements (for example) will not only produce errors in the computed distance to these sources, but also in the corresponding analysis for gravity. It would be naive to simply assume that these effects are negligible and do not require further study.

4.2.1 Measurement Noise

The expected sources of measurement noise, which are not corrected by calibration, are movement of the instrument, as well as moving and possibly time dependent massive sources in the instrument's immediate environment.

The movement of the instrument comes about as a result of the fact that the planes position will

not be fixed: the plane's orientation may vary, turbulence may cause sudden variations in altitude etc. This can produce two types of errors. First, the gradiometer will produce noisy gradient measurements. Second, the measured position of the aircraft may be inaccurate. This will in turn produce errors when the gradients are reduced and the anomalies are interpreted. These possibilities will be dealt with in turn.

As has already been mentioned, the gradiometer is unaffected by constant acceleration of the aircraft. It has been claimed that under reasonable operating conditions, the aircraft represents a *linear acceleration* environment [dMKP01]. Further, in [dMKP01], a gradiometer was mounted on a shakeable platform on the laboratory floor and extensive studies under controlled acceleration were perform. It was further claimed in [dMKP01], that the results obtained represent the best laboratory performance of any gradiometers then currently under development. The article is not clear, but the noise has an rms value of $\pm$ 3 $\cdot 5$ Eö.

4.3 The Complete Bougeur Correction: Terrain Correction

The Bougeur correction discussed in the previous section accounts for extra mass above sea level (simple Bougeur anomaly) as well as the curvature of the earth. The final correction that needs to be computed is the correction coming from the local terrain. The terrain correction can be done by approximating the topography with a digital terrain model and then calculating the gravitational attraction of the model. Even though there are two methods to compute the gravitational terrain (the Green's function based methods and the Fourier domain modelling), in this section we will restrict our discussion to the calculation of the Bougeur correction using a Green' function based method.

In modern studies of airborne gravimetry, the terrain corrections take into account all the topography out to a radius of 166.7km. This implies that it is usually valid to ignore topography beyond 166.7km and any other distant topography effect above this do not contribute significant difference. The Interpreter in the survey should be aware of such contributions and and prepare to account for them in situations requiring such precision. A rule should be developed which, given the DTM, allows one to determine how much of the terrain needs to be included to correct the gradient data.

In the terrain correction it is logical to build a detailed model of the geology of the local terrain. In this case the terrain correction is implicitly performed during the interpretation process. In this light, one may even question why the capability of performing a terrain correction is being pursued! To perform a terrain correction, one is developing the ability to forward model gradient responses from any given terrain. During this process, one is learning about the sensitivity of the gradient response of errors in the aircraft altitude and errors in the digital terrain model.

At the end of this section, algorithms to compute the terrain corrections for both gravity and gradient data are developed. The advantage of doing this is that it allows for more convincing tests of approach adopted here since terrain corrections of gravity are understood much better than the terrain correction for the gradient data.

4.3.1 Green's Function Based Methods

The Green's function method breaks the terrain down in to a set of point sources. The Green's function from each source is summed to obtain the total response from the terrain. In practice the infinite sum become an integral and is evaluated using the standard techniques. The popular way in which this can be done is to break the terrain up into rectangular prisms. In principal, any shape for the source would do as long as the analytic form of the response from the source is known. Rectangular prism are convenient because they can easily be stacked to approximate the terrain and because both the gravity and gradient response from the rectangular prism is known in closed form. In addition the rectangular prism can be model to be able to determine the complicated shape of the anomalies or underlying geology, and to be able to visualise three dimensional problem as it arises. One of the disadvantages of an employing prism is that it high accuracy is required, a large number of the prism will be required to provide a suitably accurate model of the terrain.

In contrast to the method employing rectangular prism, the so-called "stack of lamina" approach [Bla96], is particularly well suited to exploiting the way in which the digital terrain is set up. It may however, be more clumsy, if one wanted to iteratively fine tune a model for the geology, something which may be needed when an interpretation is to be performed.

The idea behind this method is to approximate each body by a stack of laminas of finite thickness. In practice, the shape of these laminas can be taken directly from the contour of equal height, from a contour of the topography of the terrain. Each contour will be represented as a set of discrete polygon samples. The response of each polygon can be computed using the Green's function of the gravitational field. This entails a triple numerical integration which is computationally expensive. The advantage of setting the model up in terms of the polygon, is that the integral can be done analytically, with the result depending only on the coordinates of the corner of the polygons. This will be amendable to the computer.

In chapter one we have discussed that the Green's function satisfies Poisson's equation

$$\nabla^2 G(\mathbf{r}) = \delta^{(3)}(\mathbf{r}). \tag{4.27}$$

For simplicity, but without loss of generality, we have located the mass point source at the origin. We have absorbed factors of mass and Newton's constant into $G(\mathbf{r})$ and will only reinstate them when necessary. Dimensional analysis tells us that if $[x] = L$, then $[\nabla] = L^{-2}$ and $\left[\delta^{(3)}\right] = L^{-3}$, from this analysis, the Green's function also holds true and obeys Poisson's equation. We will immediate write

$$G(\mathbf{r}) = \frac{\gamma}{|\mathbf{r}|} \tag{4.28}$$

The constant γ can easily be fixed by explicit computation. In term of this Green's function, the potential at position $\mathbf{r}$ due to the source with density $\rho(\mathbf{r})$ can be written as

$$U(\mathbf{r}) = \int_v d^3\mathbf{r}'\rho(\mathbf{r}')G(\mathbf{r}-\mathbf{r}') = -\gamma \int_v d^3r' \, \frac{\rho(\mathbf{r}')}{|\mathbf{r}-\mathbf{r}'|} \tag{4.29}$$

However this is not the quantity of interest. Gravity meters measure the vertical attraction of

gravity which can easily be obtained by differentiating the above formula.

$$g_z(\mathbf{r}) = -\gamma \int_v d^3r' \, \frac{\rho(\mathbf{r}')(z - z')}{|\mathbf{r} - \mathbf{r}'|^3}. \tag{4.30}$$

For the case of the gravity gradiometer considered in this report, the quantity of interest is given by

$$g_{zz}(\mathbf{r}) = -\frac{\partial}{\partial z} g_z(\mathbf{r}). \tag{4.31}$$

Next the source is decomposed into stack of laminas. Assume that each of the laminas has constant density, the above expression for g_z may be written as

$$g_z(\mathbf{r}) = \gamma \int dz' \rho(\mathbf{r}') H(\mathbf{r} - \mathbf{r}') \tag{4.32}$$

The above formula allow for a z dependent density. However, this is not used in practice. Usually, the density is to be constant. Theanomaliess then reflect the density variations. The function H(.) is defined by

$$H(\mathbf{r}) = \gamma \int dx \int dy \frac{1}{|\mathbf{r} - \mathbf{r}'|^3}. \tag{4.33}$$

The double integral can be done analytically. To perform the integration over x, note that

$$\frac{\partial}{\partial x} \left(\frac{x}{(y^2 + z^2)\sqrt{x^2 + y^2 + z^2}} \right) = \frac{1}{(x^2 + y^2 + z^2)^{3/2}}. \tag{4.34}$$

Performing the integral operation,

$$H(z - z') = \int dy \, \frac{x - x'}{((y - y')^2 + (z - z')^2)\sqrt{(x - x')^2 + (y - y')^2 + (z - z')^2}} \Bigg|_{x_1(y)}^{x_{2(y)}} \tag{4.35}$$

There is a one dimensional integral over y left to be done. At each y there are two x values $x_1(y)$ and $x_1(y)$, which represent paths around the lamina. The observation makes it clear that the remaining integral can be view as in the counter-clockwise direction around the parameter of the lamina.

$$H(z - z') = \oint dy \frac{x - x'}{((y - y')^2 + (z - z')^2)\sqrt{(x - x')^2 + (y - y')^2 + (z - z')^2}} \tag{4.36}$$

The above integration depends crucially on the orientation of the coordinate system of the parameter of lamina. The orientation assume here is shown below. One have a choice to decide what orientation to take. For another orientation see below. In the above orientation the integral should be performed clockwise direction around the parameter of the lamina. The perimeter of the lamina is defined by a set of discrete points (the vertices of the polygon) which are specify by the digital terrain model. Thus the above path integration can be replaced by integration of set of straight line segments, of being a side of the polygon. See figure(4.3.1)

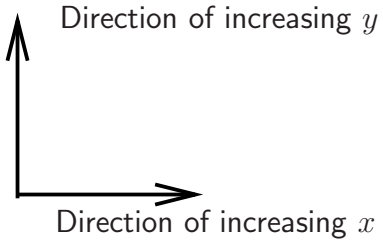

Figure 4.5: With the above orientation of the x and y axes, one should integrate around the perimeter of the lamina in a counter-clockwise direction.

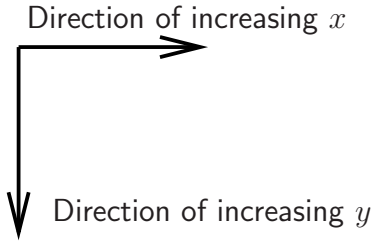

Figure 4.6: With the above orientation of the x and y axes, one should integrate around the perimeter of the lamina in a clockwise direction.

With this approximation (the polygon has M sides)

$$H(z-z') = \sum_{m=1}^{M} \int_{y_m}^{y_{m+1}} dy \frac{x-x'}{((y-y')^2+(z-z')^2)\sqrt{(x-x')^2+(y-y')^2+(z-z')^2}} \quad (4.37)$$

with y_m and y_{m+1} the y coordinate of the m^{th} side of the polygon and

$$x - x' = \alpha_m(y-y') + \beta_m, \quad : \alpha_m = \frac{x_{m+1}-x'_m}{y_{m+1}-y_m},$$

$$\beta_m = \frac{(x_m-x')(y_{m+1}-y') - (x_{m+1}-x')(y_m-y')}{y_{m+1}-y_m}$$

According from [grant and west [99]]the following analytic result for $H(z)$ is obtained

$$(z-z')H(z-z') = \sum_{m=1}^{M} \left(\arctan\left[\frac{w_m}{\tau_m}\right] - \arctan\left[\frac{\eta_m}{k_m}\right] \right), \quad (4.38)$$

from the above equation we can write

$$\begin{aligned}
w_m &= (z-z)(\beta_m(y'-y_{m+1}) - \alpha_m(z'-z), \\
\tau_m &= (x'-x_{m+1})\left[(1+\alpha_m^2)(z'-z)^2+\beta_m^2\right] \\
&\quad - \left(\alpha^2(z'-z)^2+\beta_m^2\right)\sqrt{(x_{m+1}+x')^2+(y_{m+1}-y')^2+(z'-z)^2}, \\
\eta_m &= (z'-z)\left(\beta_m(y_{m+1}-y') - \alpha_m(z'-z)^2\right), \\
k_m &= (x'-x_m)\left[(1+\alpha_m^2)(z'-z)^2+\beta_m^2\right] \\
&\quad - \left(\alpha_m^2((z'-z)^2+\beta_m^2\right)\sqrt{(x_m-x')^2+(y_{m+1}-y')^2+(z'-z)^2}.
\end{aligned}$$

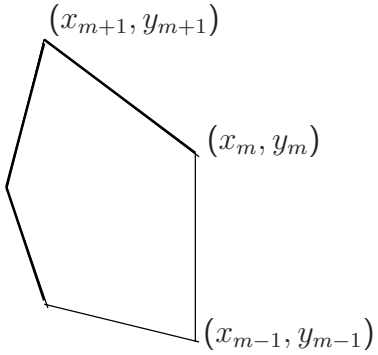

Figure 4.7: Labelling of the vertices of the polygons consistent with the conventions for axes orientation in this report.

The final (z) integration has been performed in [Plo76] and is given as

$$g_z = \gamma\rho s_m \sum_{i=1}^{M} \left[\epsilon(P) A[z_+ - z_-] + z_+ \left[\arctan \frac{z_+ d_i}{PR_{i,i+1}} - \arctan \frac{z_+ d_{i+1}}{PR_{i+1,i+1}} \right] \right.$$
$$\left. -z_- \left[\arctan \frac{z_- d_i}{PR_{ii}} - \arctan \frac{z_- d_{i+1}}{PR_{i+1,i}} \right] - P \log \frac{(R_{i+1,i+1} + d_{i+1})(R_{ii} + d_i)}{(R_{i,i+1} + d_i)(R_{i+1,i} + d_{i+1})} \right] \tag{4.39}$$

In the above equation let

$$A = \arccos \frac{x_i x_{i+1} + y_i y_{i+1}}{r_i r_{i+1}}, \quad : \Delta y = y_{i+1} - y_i, \quad : \Delta x = x_{i+1} - x_i$$
$$\Delta s = \sqrt{(\Delta x)^2 + (\Delta y)^2} \quad : S = \frac{\Delta x}{\Delta s,} \quad : C = \frac{\Delta y}{\Delta s}, \quad : d_k = x_k S + y_k C,$$
$$P = x_k C + y_k S, \quad : R_{jk} = \sqrt{r_k^2 + z_j^2}. \quad : r_k = \sqrt{x_k^2 + y_k^2}.$$

The points (x, y) are on order set of (x, y) coordinates on the boundary of the polygon ; z_+ is elevation of the polygon ;z_- is the elevation of the bottom of the polygon. The symbol $s_m = 1$ if the center of the mass of the prism is below the observation point ad $s_m = -1$ if the center of the mass of the prism is above the observation point. The last comment is important : *By appropriately choosing s_m the above formula correction gives the response to a polygon even if the polygon lies at a higher elevation then the observation point!*

Next consider the terrain correction to the gradient. This correction is easily obtained by differentiating the above result. One obtains

$$g_{zz} = \gamma\rho s_m \sum_{i=1}^{M} \left[\arctan \frac{z_+ d_i}{PR_{i,i+1}} - \arctan \frac{z_+ d_{i+1}}{PR_{i+1,i+1}} - \left(\arctan \frac{z_- d_i}{PR_{ii}} - \arctan \frac{z_- d_{i+1}}{PR_{i+1,i}} \right) \right] \tag{4.40}$$

The arctan(.) function is not single valued. This raises the question as to which sheet the value should lies on. This (possible) problem can easily be dealt with, by using the arctan identities.

$$\arctan(A) - \arctan(B) = \arctan\left(\frac{A-B}{1+AB}\right) \tag{4.41}$$

and always evaluating this last arctan on its principle domain, the ambiguity is resolved. From the above equation only two arctan evaluation is necessary for the gravity response and only one arctan evaluation in the case of the gradient response. This is to reduce the run time of the code.

Although the derivation in this section was implicitly aimed towards solving the problem of terrain corrections, it is clear that the algorithms developed can be used to generate synthetic data. By allowing the density ρ to vary between different lamina of different prisms, it is possible to model any procribed ore body. The advantage of synthetic data is that it allows a systematic study of algorithms that will be used to process the measured data in controlled environments were the exact structure of the anomalies is know.

The algorithms developed is amenable to computer simulations. See the Appendix for some examples.

5. Conclusion

We began by introducing the concept of the Green's function and after that we derived the Green's function for Poisson's equation after imposing suitable boundary conditions. Poisson's equation describes the gravitational potential in a region where a mass density distribution may be present.

We pointed out that in a geophysical survey (which is aimed at determining the mass density distribution in the local terrain), the vertical component of the acceleration g_z due to gravity and the vertical gravity gradient g_{zz} are usually measured. Both these quantities were shown to be harmonic functions, i.e., they obey Laplace's equation in source-free regions, a property which we suggested may be exploited to filter out noise from the measurement data. We showed that even though there exist other components of the acceleration due to gravity (two others) and the gravity gradient (eight others) which the geophysical survey does not measure, it is possible using suitable boundary conditions to compute, with only these two types of measurements, the gravitational potential up to an additive constant.

The Green's functions corresponding to g_z and g_{zz} were also computed. Following this, an analytic expression for g_{zz} in terms of the local terrain mass density distribution was obtained, and by converting this expression from a volume integral to a surface integral we provided an alternative description for g_{zz} namely that it may be considered to be the "gravitational field" due to "gravitational dipoles" located all over the surface of the digital terrain model representing the local terrain. This alternative description enables us to employ the Green's function for g_z to compute g_{zz}.

We also discussed the various corrections, or anomalies associated with measuring $g_z z$ and g_z, demonstrating that most of the corrections applicable to g_z measurements are not applicable to g_{zz} measurements. However, we hinted that there are most likely new corrections applicable to g_{zz} readings but which are not applicable to g_z readings. The calculations of g_{zz} due to the local terrain are actually part of a well-known type of correction known as the Bouger correction. By approximating the terrain by a composition of polygonal prisms each of constant density we obtained a numerical expression which could aid in the efficient computation of the convolution integrals involving the Green's function for the computation of g_{zz}.

The essay opens doors for further research, especially into the problem of removing noise from gravity gradient readings. Current literature offers other methods which are not based on using Green's functions for computing g_{zz} given a digital terrain model. One of such methods is the Fourier Domain Modelling. With the usage of the well-known and very efficient Fast Fourier Transform (FFT) routines, this method may prove to be even more efficient than the one presented in this essay.

Appendix A. Graphical Representation of g_{zz} plot from computer stimulation

Below are results of simulations done using Equation (4.40). All constants were set to unity. The plots are included here to illustrate how the g_{zz} field conforms to the shape of the mass density distribution that causes it.

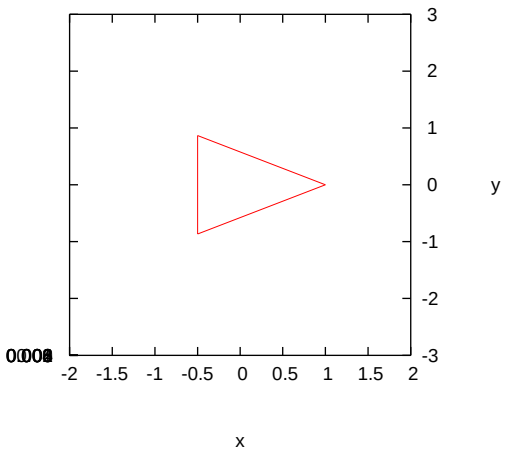

Figure A.1: Triangular density distribution with a thickness of 0.5 and top elevation on the $z = 0$ plane.

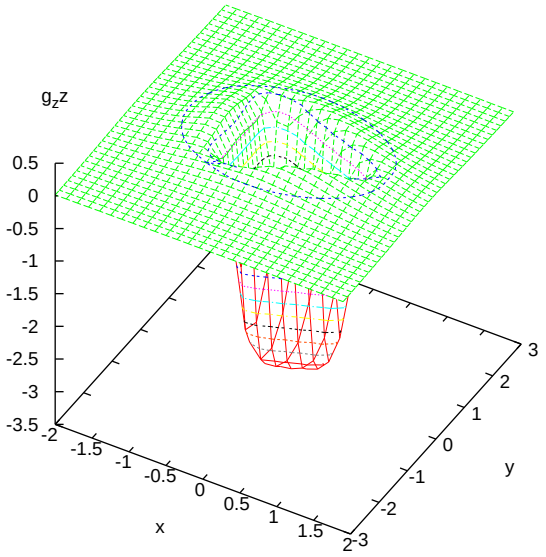

Figure A.2: Surface plot of g_{zz} for the triangular mass density distribution shown in Figure (A.1). The values of g_{zz} were calculated along the $z = 0.125$ plane.

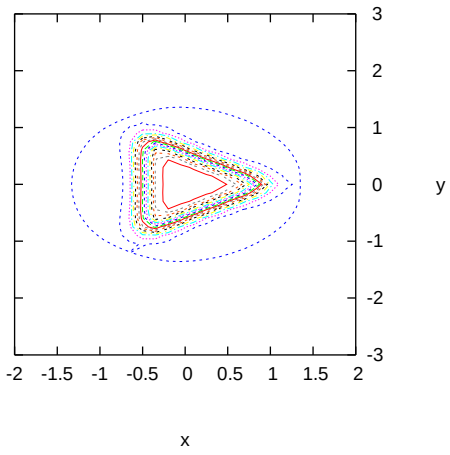

Figure A.3: Contour Plot of g_{zz} for the triangular mass density distribution shown in Figure (A.1). The values of g_{zz} were calculated along the $z = 0.125$ plane.

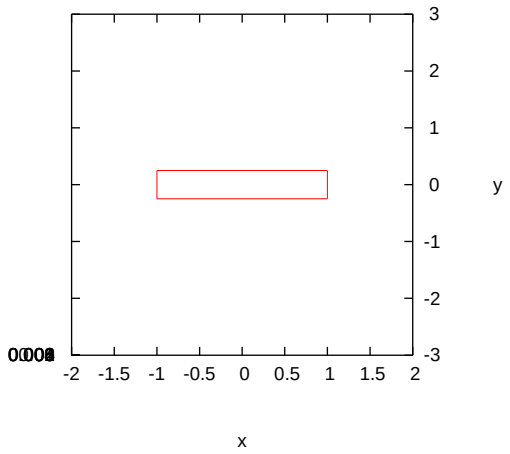

Figure A.4: Rectangular density distribution with a thickness of 0.5 and top elevation on the $z = 0$ plane.

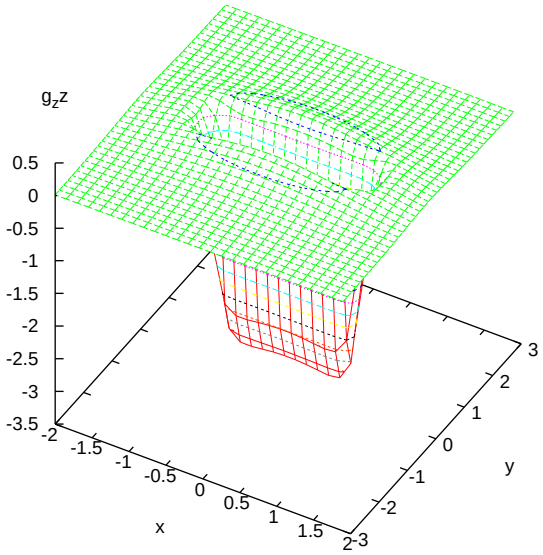

Figure A.5: Surface plot of g_{zz} for the rectangular mass density distribution shown in Figure (A.4). The values of g_{zz} were calculated along the $z = 0.125$ plane.

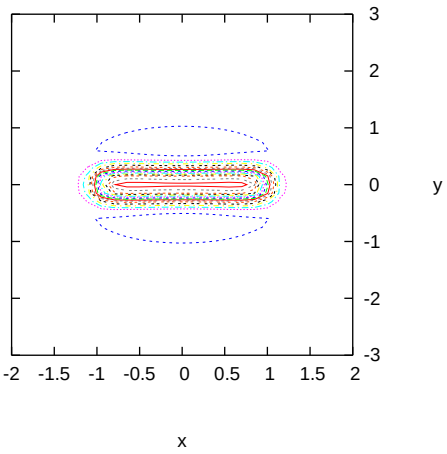

Figure A.6: Contour plot of g_{zz} for the rectangular mass density distribution shown in Figure (A.4). The values of g_{zz} were calculated along the $z = 0.125$ plane.

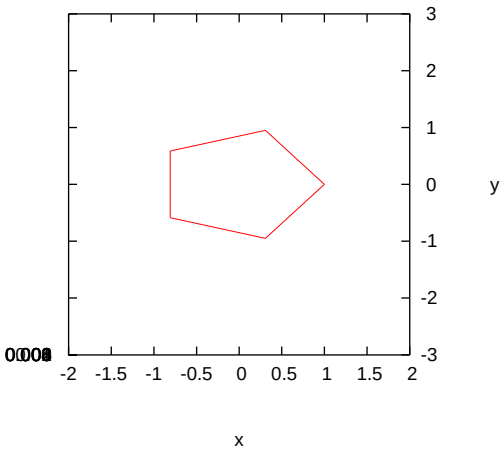

Figure A.7: Pentagonal density distribution with a thickness of 0.5 and top elevation on the $z = 0$ plane.

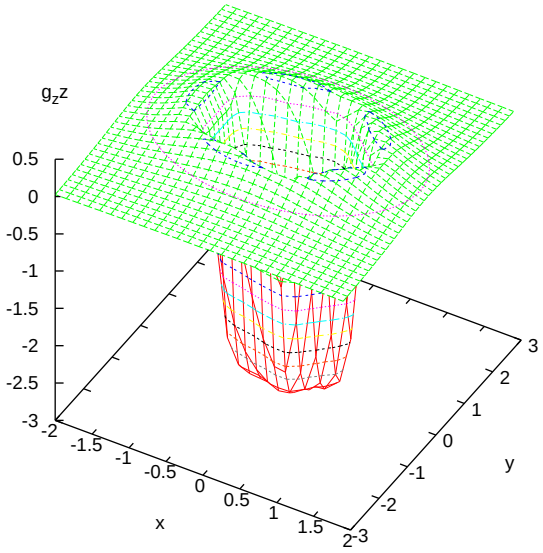

Figure A.8: Surface plot of g_{zz} for the pentagonal mass density distribution shown in Figure (A.7). The values of g_{zz} were calculated along the $z = 0.125$ plane.

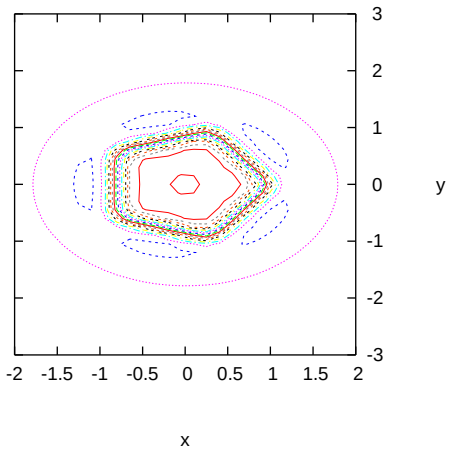

Figure A.9: Contour plot of g_{zz} for the pentagonal mass density distribution shown in Figure (A.7). The values of g_{zz} were calculated along the $z = 0.125$ plane.

Appendix B. Python Code Used to do the Simulation

```
from __future__ import division
from scipy import *
import MA
import Gnuplot

## NUMERICAL QUADRATURE VERSION
##############################################

def func2d(y0, x0, xx, yy, zz, z0):
    return 1 / ( (xx - x0)**2 + (yy - y0)**2 + (zz - z0)**2)**(3/2)

def hfunc(x):
    return 0.25

def gfunc(x):
    return -0.25

def xy_integral(xxP, xxM, xx, yy, zz, z0):
    q = integrate.dblquad(func2d, xxM, xxP, gfunc, hfunc, args=(xx, yy, zz, z0))
    return q[0]

def compute_ana_gzz2(xx, yy, zz, xxP, yyP, zzP, xM, yM, zM):
    gzz = (zz - zzP) * xy_integral(xxP, xM, xx, yy, zz, zzP) - (zz -  zM) * xy_integral(xxP, xM, xx, yy, zz, zM)
    return -gzz


#  NUMERICAL SUMMATION VERSION
##############################################


gp = Gnuplot.Gnuplot(persist = 1)
sM = 1
gamma = 1
rho = 1

# polygon vertices
filename = raw_input("Enter filename with DTM data: ")
data = io.array_import.read_array(filename)
xP = data[1:,0]
yP = data[1:,1]
zT = data[0,0]
zB = data[0,1]
zP = array([zT, zB])
N = len(xP)

x = 0
y = 0
z = 0

obsPoint = array([x, y, z])

def compute_gzz(obsPoint):
    # size M + 1 arrays
    x = xP - obsPoint[0]
    y = yP - obsPoint[1]
    z = zP - obsPoint[2]

    # size M+1 arrays
    dx = concatenate((x[1:] - x[0:-1], [x[1] - x[0]]))
    dy = concatenate((y[1:] - y[0:-1], [y[1] - y[0]]))
    ds = sqrt(dx**2 + dy**2)
```

```
    S = dx    #/ ds
    C = dy    #/ ds

    # size M arrays
    d = x[0:-1] * S[0:-1] + y[0:-1] * C[0:-1]
    d1 = x[1:] * S[0:-1] + y[1:] * C[0:-1]
    PP = x[0:-1] * C[0:-1] - y[0:-1] * S[0:-1]
    P = PP

    r = sqrt(x**2 + y**2)
    RR = sqrt(r**2 + reshape(z, (2,1))**2)
    R0 = RR[:,0:-1]
    R1 = RR[:,1:]

    numer1 = z[0] * P * (d * R1[0, :] - d1 * R0[0, :])
    numer2 = z[1] * P * (d * R1[1, :] - d1 * R0[1, :])
    denom1 = (P**2 * R1[0, :] * R0[0, :] + z[0]**2 * d1 * d)
    denom2 = (P**2 * R0[1, :] * R1[1, :] + z[1]**2 * d1 * d)

    gzz = gamma*rho*sM*sum(arctan2(numer1*denom2-numer2*denom1, numer1*numer2 + denom1*denom2))
    return gzz


print compute_gzz([5,5,10])


Plane_limitXmin = -2
Plane_limitXmax = 2

Plane_limitYmin = -3
Plane_limitYmax = 3

PlaneHeight = 0.125
z = PlaneHeight

delta_x = 0.15
delta_y = 0.15

Xrng = arange(Plane_limitXmin, Plane_limitXmax + delta_x/2, delta_x)
Yrng = arange(Plane_limitYmin, Plane_limitYmax + delta_y/2, delta_y)
xlen = len(Xrng)
ylen = len(Yrng)
gzz = zeros((xlen, ylen), Float)

i = 0
while i < xlen:
    j = 0
    x = Xrng[i]
    while j < ylen:
        y = Yrng[j]
        obsPoint = array([x, y, z])
        gzz[i,j] = compute_gzz(obsPoint)
        #gzz[i,j] = compute_ana_gzz2(x,y,z,1.0,1,0,-1.0,-1,-0.5)  # the quadrature version
        j += 1
    i += 1

gp.set_range('xrange',(Plane_limitXmin, Plane_limitXmax))
gp.set_range('yrange',(Plane_limitYmin, Plane_limitYmax))

gp('set hidden')
gp('set ticslevel 0')
gp('set view 50, 30')
gp('set surface')
gp('set contour surface')
gp('set cntrparam levels auto 20')
gp('set key off')
gp('set xlabel "x"')
```

```
gp('set ylabel "y"')
gp('set zlabel "g_zz"')
gp('set size square')

gzzdata = Gnuplot.GridData(gzz, xvals = Xrng, yvals = Yrng, with = "lines")
polygondata = Gnuplot.Data(xP, yP, zT*ones((N,),Float), with = 'filledcurve')
gp.splot(gzzdata)
gp.hardcopy(filename=filename[0:-4] + "_gzz_surface.eps",terminal="postscript", eps = True, color = True)

gp('set terminal x11 2')
gp('set view 0, 0')
gp('unset surface')
gp('set contour base')
gp('set cntrparam levels auto 20')
gp('set key off')
gp.splot(gzzdata)
gp.hardcopy(filename=filename[0:-4] + "_gzz_contour.eps",terminal="postscript", eps = True, color = True)

gp('set terminal x11 3')
gp('set xlabel "x"')
gp('set ylabel "y"')
gp('set surface')
gp('unset contour ')
gp('unset zlabel')
gp('unset axis z')
gp.set_range('zrange',(0, 0.01))
gp.splot(polygondata)
gp.hardcopy(filename=filename[0:-4] + "_density.eps",terminal="postscript", eps = True, color = True)
```

Acknowledgement

I will like to send my profound gratitude to the AIMS family: Tutors, Students, Administrators and Friends, for their contributions throughout my stay at AIMS. In time of of obstacles they were always willing to answer to my call especially, Mr. Henry Amuasi who spent his precious time willing to clarify and work side by side with me during my essay phase. I also extend my best warmest thanks and appreciation to my supervisors, Prof. Robert de Mello Koch and Prof. Neil Pendock, for their contributions in exposing me to research methodology.

Bibliography

[Bla96] R.J. Blakely, *Potential Theory in Gravity and Magnetic Applications*, Cambridge University Press, 1996.

[dMKP01] Robert de Mello Koch and Neil Pendock, *Potential fields and gradients of potential field*, 2001.

[Hil02] Kearey Brooks Hill, *An Interduction to Geophysical Exploration*, Iowa state University press, 2002.

[Par90] J. Parmentola, *The gravity gradiometer as a verification tool*, Science and Global Security **2** (1990), 43–57.

[Plo76] D. Plouff, *Gravity and magnetic field of polygonal prisms and application to magnetic terrain corrections*, Geophysics **41** (1976), 727–41.

[RHB03] K.F Riley, M.P Hobson, and S.J Bence, *Mathematical Methods for Physics and Engineering*, Press syndicate of the university of Cambridge, 2003.

[Wil02] L. William, *Fundamentals of Geophysics*, Cambidge University press, 2002.